

Measurement of CP asymmetries and branching fractions in charmless two-body B -meson decays to pions and kaons

J. P. Lees,¹ V. Poireau,¹ V. Tisserand,¹ J. Garra Tico,² E. Grauges,² A. Palano,^{3a,3b} G. Eigen,⁴ B. Stugu,⁴ D. N. Brown,⁵ L. T. Kerth,⁵ Yu. G. Kolomensky,⁵ G. Lynch,⁵ H. Koch,⁶ T. Schroeder,⁶ D. J. Asgeirsson,⁷ C. Hearty,⁷ T. S. Mattison,⁷ J. A. McKenna,⁷ R. Y. So,⁷ A. Khan,⁸ V. E. Blinov,⁹ A. R. Buzykaev,⁹ V. P. Druzhinin,⁹ V. B. Golubev,⁹ E. A. Kravchenko,⁹ A. P. Onuchin,⁹ S. I. Serednyakov,⁹ Yu. I. Skovpen,⁹ E. P. Solodov,⁹ K. Yu. Todyshev,⁹ A. N. Yushkov,⁹ M. Bondioli,¹⁰ D. Kirkby,¹⁰ A. J. Lankford,¹⁰ M. Mandelkern,¹⁰ H. Atmacan,¹¹ J. W. Gary,¹¹ F. Liu,¹¹ O. Long,¹¹ G. M. Vitug,¹¹ C. Campagnari,¹² T. M. Hong,¹² D. Kovalskyi,¹² J. D. Richman,¹² C. A. West,¹² A. M. Eisner,¹³ J. Kroseberg,¹³ W. S. Lockman,¹³ A. J. Martinez,¹³ B. A. Schumm,¹³ A. Seiden,¹³ D. S. Chao,¹⁴ C. H. Cheng,¹⁴ B. Echenard,¹⁴ K. T. Flood,¹⁴ D. G. Hitlin,¹⁴ P. Ongmongkolkul,¹⁴ F. C. Porter,¹⁴ A. Y. Rakitin,¹⁴ R. Andreassen,¹⁵ Z. Huard,¹⁵ B. T. Meadows,¹⁵ M. D. Sokoloff,¹⁵ L. Sun,¹⁵ P. C. Bloom,¹⁶ W. T. Ford,¹⁶ A. Gaz,¹⁶ U. Nauenberg,¹⁶ J. G. Smith,¹⁶ S. R. Wagner,¹⁶ R. Ayad,^{17,*} W. H. Toki,¹⁷ B. Spaan,¹⁸ K. R. Schubert,¹⁹ R. Schwierz,¹⁹ D. Bernard,²⁰ M. Verderi,²⁰ P. J. Clark,²¹ S. Playfer,²¹ D. Bettoni,^{22a} C. Bozzi,^{22a} R. Calabrese,^{22a,22b} G. Cibinetto,^{22a,22b} E. Fioravanti,^{22a,22b} I. Garzia,^{22a,22b} E. Luppi,^{22a,22b} M. Munerato,^{22a,22b} M. Negrini,^{22a,22b} L. Piemontese,^{22a} V. Santoro,^{22a} R. Baldini-Ferroli,²³ A. Calcaterra,²³ R. de Sangro,²³ G. Finocchiaro,²³ P. Patteri,²³ I. M. Peruzzi,^{23,†} M. Piccolo,²³ M. Rama,²³ A. Zallo,²³ R. Contri,^{24a,24b} E. Guido,^{24a,24b} M. Lo Vetere,^{24a,24b} M. R. Monge,^{24a,24b} S. Passaggio,^{24a} C. Patrignani,^{24a,24b} E. Robutti,^{24a} B. Bhuyan,²⁵ V. Prasad,²⁵ C. L. Lee,²⁶ M. Morii,²⁶ A. J. Edwards,²⁷ A. Adametz,²⁸ U. Uwer,²⁸ H. M. Lacker,²⁹ T. Lueck,²⁹ P. D. Dauncey,³⁰ P. K. Behera,³¹ U. Mallik,³¹ C. Chen,³² J. Cochran,³² W. T. Meyer,³² S. Prell,³² A. E. Rubin,³² A. V. Gritsan,³³ Z. J. Guo,³³ N. Arnaud,³⁴ M. Davier,³⁴ D. Derkach,³⁴ G. Grosdidier,³⁴ F. Le Diberder,³⁴ A. M. Lutz,³⁴ B. Malaescu,³⁴ P. Roudeau,³⁴ M. H. Schune,³⁴ A. Stocchi,³⁴ G. Wormser,³⁴ D. J. Lange,³⁵ D. M. Wright,³⁵ C. A. Chavez,³⁶ J. P. Coleman,³⁶ J. R. Fry,³⁶ E. Gabathuler,³⁶ D. E. Hutchcroft,³⁶ D. J. Payne,³⁶ C. Touramanis,³⁶ A. J. Bevan,³⁷ F. Di Lodovico,³⁷ R. Sacco,³⁷ M. Sigamani,³⁷ G. Cowan,³⁸ D. N. Brown,³⁹ C. L. Davis,³⁹ A. G. Denig,⁴⁰ M. Fritsch,⁴⁰ W. Gradl,⁴⁰ K. Griessinger,⁴⁰ A. Hafner,⁴⁰ E. Prencipe,⁴⁰ R. J. Barlow,^{41,‡} G. Jackson,⁴¹ G. D. Lafferty,⁴¹ E. Behn,⁴² R. Cenci,⁴² B. Hamilton,⁴² A. Jawahery,⁴² D. A. Roberts,⁴² C. Dallapiccola,⁴³ R. Cowan,⁴⁴ D. Dujmic,⁴⁴ G. Sciolla,⁴⁴ R. Cheaib,⁴⁵ D. Lindemann,⁴⁵ P. M. Patel,^{45,§} S. H. Robertson,⁴⁵ P. Biassoni,^{46a,46b} N. Neri,^{46a} F. Palombo,^{46a,46b} S. Stracka,^{46a,46b} L. Cremaldi,⁴⁷ R. Godang,^{47,||} R. Kroeger,⁴⁷ P. Sonnek,⁴⁷ D. J. Summers,⁴⁷ X. Nguyen,⁴⁸ M. Simard,⁴⁸ P. Taras,⁴⁸ G. De Nardo,^{49a,49b} D. Monorchio,^{49a,49b} G. Onorato,^{49a,49b} C. Sciacca,^{49a,49b} M. Martinelli,⁵⁰ G. Raven,⁵⁰ C. P. Jessop,⁵¹ J. M. LoSecco,⁵¹ W. F. Wang,⁵¹ K. Honscheid,⁵² R. Kass,⁵² J. Brau,⁵³ R. Frey,⁵³ N. B. Sinev,⁵³ D. Strom,⁵³ E. Torrence,⁵³ E. Feltresi,^{54a,54b} N. Gagliardi,^{54a,54b} M. Margoni,^{54a,54b} M. Morandin,^{54a} M. Posocco,^{54a} M. Rotondo,^{54a} G. Simi,^{54a} F. Simonetto,^{54a,54b} R. Stroili,^{54a,54b} S. Akar,⁵⁵ E. Ben-Haim,⁵⁵ M. Bomben,⁵⁵ G. R. Bonneaud,⁵⁵ H. Briand,⁵⁵ G. Calderini,⁵⁵ J. Chauveau,⁵⁵ O. Hamon,⁵⁵ Ph. Leruste,⁵⁵ G. Marchiori,⁵⁵ J. Ocariz,⁵⁵ S. Sitt,⁵⁵ M. Biasini,^{56a,56b} E. Manoni,^{56a,56b} S. Pacetti,^{56a,56b} A. Rossi,^{56a,56b} C. Angelini,^{57a,57b} G. Batignani,^{57a,57b} S. Bettarini,^{57a,57b} M. Carpinelli,^{57a,57b,||} G. Casarosa,^{57a,57b} A. Cervelli,^{57a,57b} F. Forti,^{57a,57b} M. A. Giorgi,^{57a,57b} A. Lusiani,^{57a,57c} B. Oberhof,^{57a,57b} E. Paoloni,^{57a,57b} A. Perez,^{57a} G. Rizzo,^{57a,57b} J. J. Walsh,^{57a} D. Lopes Pegna,⁵⁸ J. Olsen,⁵⁸ A. J. S. Smith,⁵⁸ A. V. Telnov,⁵⁸ F. Anulli,^{59a} R. Faccini,^{59a,59b} F. Ferrarotto,^{59a} F. Ferroni,^{59a,59b} M. Gaspero,^{59a,59b} L. Li Gioi,^{59a} M. A. Mazzoni,^{59a} G. Piredda,^{59a} C. Büniger,⁶⁰ O. Grünberg,⁶⁰ T. Hartmann,⁶⁰ T. Leddig,⁶⁰ H. Schröder,^{60,§} C. Voss,⁶⁰ R. Waldi,⁶⁰ T. Auye, ⁶¹ E. O. Olaiya,⁶¹ F. F. Wilson,⁶¹ S. Emery,⁶² G. Hamel de Monchenault,⁶² G. Vasseur,⁶² Ch. Yèche,⁶² D. Aston,⁶³ D. J. Bard,⁶³ R. Bartoldus,⁶³ J. F. Benitez,⁶³ C. Cartaro,⁶³ M. R. Convery,⁶³ J. Dorfan,⁶³ G. P. Dubois-Felsmann,⁶³ W. Dunwoodie,⁶³ M. Ebert,⁶³ R. C. Field,⁶³ M. Franco Sevilla,⁶³ B. G. Fulsom,⁶³ A. M. Gabareen,⁶³ M. T. Graham,⁶³ P. Grenier,⁶³ C. Hast,⁶³ W. R. Innes,⁶³ M. H. Kelsey,⁶³ P. Kim,⁶³ M. L. Kocian,⁶³ D. W. G. S. Leith,⁶³ P. Lewis,⁶³ B. Lindquist,⁶³ S. Luitz,⁶³ V. Luth,⁶³ H. L. Lynch,⁶³ D. B. MacFarlane,⁶³ D. R. Muller,⁶³ H. Neal,⁶³ S. Nelson,⁶³ M. Perl,⁶³ T. Pulliam,⁶³ B. N. Ratcliff,⁶³ A. Roodman,⁶³ A. A. Salnikov,⁶³ R. H. Schindler,⁶³ A. Snyder,⁶³ D. Su,⁶³ M. K. Sullivan,⁶³ J. Va'vra,⁶³ A. P. Wagner,⁶³ W. J. Wisniewski,⁶³ M. Wittgen,⁶³ D. H. Wright,⁶³ H. W. Wulsin,⁶³ C. C. Young,⁶³ V. Ziegler,⁶³ W. Park,⁶⁴ M. V. Purohit,⁶⁴ R. M. White,⁶⁴ J. R. Wilson,⁶⁴ A. Randle-Conde,⁶⁵ S. J. Sekula,⁶⁵ M. Bellis,⁶⁶ P. R. Burchat,⁶⁶ T. S. Miyashita,⁶⁶ M. S. Alam,⁶⁷ J. A. Ernst,⁶⁷ R. Gorodeisky,⁶⁸ N. Guttman,⁶⁸ D. R. Peimer,⁶⁸ A. Soffer,⁶⁸ P. Lund,⁶⁹ S. M. Spanier,⁶⁹ J. L. Ritchie,⁷⁰ A. M. Ruland,⁷⁰ R. F. Schwitters,⁷⁰ B. C. Wray,⁷⁰ J. M. Izen,⁷¹ X. C. Lou,⁷¹ F. Bianchi,^{72a,72b} D. Gamba,^{72a,72b} L. Lanceri,^{73a,73b} L. Vitale,^{73a,73b} F. Martinez-Vidal,⁷⁴ A. Oyangueren,⁷⁴ H. Ahmed,⁷⁵ J. Albert,⁷⁵ Sw. Banerjee,⁷⁵ F. U. Bernlochner,⁷⁵ H. H. F. Choi,⁷⁵ G. J. King,⁷⁵ R. Kowalewski,⁷⁵ M. J. Lewczuk,⁷⁵ I. M. Nugent,⁷⁵ J. M. Roney,⁷⁵ R. J. Sobie,⁷⁵ N. Tasneem,⁷⁵ T. J. Gershon,⁷⁶ P. F. Harrison,⁷⁶ T. E. Latham,⁷⁶ E. M. T. Puccio,⁷⁶ H. R. Band,⁷⁷ S. Dasu,⁷⁷ Y. Pan,⁷⁷ R. Prepost,⁷⁷ and S. L. Wu⁷⁷

(BABAR Collaboration)

- ¹Laboratoire d'Annecy-le-Vieux de Physique des Particules (LAPP), Université de Savoie, CNRS/IN2P3, F-74941 Annecy-Le-Vieux, France
- ²Facultat de Física, Departament ECM, Universitat de Barcelona, E-08028 Barcelona, Spain
- ^{3a}INFN Sezione di Bari, I-70126 Bari, Italy
- ^{3b}Dipartimento di Fisica, Università di Bari, I-70126 Bari, Italy
- ⁴Institute of Physics, University of Bergen, N-5007 Bergen, Norway
- ⁵Lawrence Berkeley National Laboratory and University of California, Berkeley, California 94720, USA
- ⁶Institut für Experimentalphysik I, Ruhr Universität Bochum, D-44780 Bochum, Germany
- ⁷University of British Columbia, Vancouver, British Columbia, Canada V6T 1Z1
- ⁸Brunel University, Uxbridge, Middlesex UB8 3PH, United Kingdom
- ⁹Budker Institute of Nuclear Physics, Novosibirsk 630090, Russia
- ¹⁰University of California at Irvine, Irvine, California 92697, USA
- ¹¹University of California at Riverside, Riverside, California 92521, USA
- ¹²University of California at Santa Barbara, Santa Barbara, California 93106, USA
- ¹³Institute for Particle Physics, University of California at Santa Cruz, Santa Cruz, California 95064, USA
- ¹⁴California Institute of Technology, Pasadena, California 91125, USA
- ¹⁵University of Cincinnati, Cincinnati, Ohio 45221, USA
- ¹⁶University of Colorado, Boulder, Colorado 80309, USA
- ¹⁷Colorado State University, Fort Collins, Colorado 80523, USA
- ¹⁸Fakultät Physik, Technische Universität Dortmund, D-44221 Dortmund, Germany
- ¹⁹Institut für Kern- und Teilchenphysik, Technische Universität Dresden, D-01062 Dresden, Germany
- ²⁰Laboratoire Leprince-Ringuet, Ecole Polytechnique, CNRS/IN2P3, F-91128 Palaiseau, France
- ²¹University of Edinburgh, Edinburgh EH9 3JZ, United Kingdom
- ^{22a}INFN Sezione di Ferrara, I-44100 Ferrara, Italy
- ^{22b}Dipartimento di Fisica, Università di Ferrara, I-44100 Ferrara, Italy
- ²³INFN Laboratori Nazionali di Frascati, I-00044 Frascati, Italy
- ^{24a}INFN Sezione di Genova, I-16146 Genova, Italy
- ^{24b}Dipartimento di Fisica, Università di Genova, I-16146 Genova, Italy
- ²⁵Indian Institute of Technology Guwahati, Guwahati, Assam 781 039, India
- ²⁶Harvard University, Cambridge, Massachusetts 02138, USA
- ²⁷Harvey Mudd College, Claremont, California 91711, USA
- ²⁸Physikalisches Institut, Universität Heidelberg, Philosophenweg 12, D-69120 Heidelberg, Germany
- ²⁹Institut für Physik, Humboldt-Universität zu Berlin, Newtonstraße 15, D-12489 Berlin, Germany
- ³⁰Imperial College London, London, SW7 2AZ, United Kingdom
- ³¹University of Iowa, Iowa City, Iowa 52242, USA
- ³²Iowa State University, Ames, Iowa 50011-3160, USA
- ³³Johns Hopkins University, Baltimore, Maryland 21218, USA
- ³⁴Laboratoire de l'Accélérateur Linéaire, IN2P3/CNRS et Université Paris-Sud 11, Centre Scientifique d'Orsay, B. P. 34, F-91898 Orsay Cedex, France
- ³⁵Lawrence Livermore National Laboratory, Livermore, California 94550, USA
- ³⁶University of Liverpool, Liverpool L69 7ZE, United Kingdom
- ³⁷Queen Mary, University of London, London, E1 4NS, United Kingdom
- ³⁸University of London, Royal Holloway and Bedford New College, Egham, Surrey TW20 0EX, United Kingdom
- ³⁹University of Louisville, Louisville, Kentucky 40292, USA
- ⁴⁰Institut für Kernphysik, Johannes Gutenberg-Universität Mainz, D-55099 Mainz, Germany
- ⁴¹University of Manchester, Manchester M13 9PL, United Kingdom
- ⁴²University of Maryland, College Park, Maryland 20742, USA
- ⁴³University of Massachusetts, Amherst, Massachusetts 01003, USA
- ⁴⁴Laboratory for Nuclear Science, Massachusetts Institute of Technology, Cambridge, Massachusetts 02139, USA
- ⁴⁵McGill University, Montréal, Québec, Canada H3A 2T8
- ^{46a}INFN Sezione di Milano, I-20133 Milano, Italy
- ^{46b}Dipartimento di Fisica, Università di Milano, I-20133 Milano, Italy
- ⁴⁷University of Mississippi, University, Mississippi 38677, USA
- ⁴⁸Physique des Particules, Université de Montréal, Montréal, Québec, Canada H3C 3J7
- ^{49a}INFN Sezione di Napoli, I-80126 Napoli, Italy
- ^{49b}Dipartimento di Scienze Fisiche, Università di Napoli Federico II, I-80126 Napoli, Italy
- ⁵⁰NIKHEF, National Institute for Nuclear Physics and High Energy Physics, NL-1009 DB Amsterdam, The Netherlands

⁵¹University of Notre Dame, Notre Dame, Indiana 46556, USA⁵²Ohio State University, Columbus, Ohio 43210, USA⁵³University of Oregon, Eugene, Oregon 97403, USA^{54a}INFN Sezione di Padova, I-35131 Padova, Italy^{54b}Dipartimento di Fisica, Università di Padova, I-35131 Padova, Italy⁵⁵Laboratoire de Physique Nucléaire et de Hautes Energies, IN2P3/CNRS, Université Pierre et Marie Curie-Paris6, Université Denis Diderot-Paris7, F-75252 Paris, France^{56a}INFN Sezione di Perugia, I-06100 Perugia, Italy^{56b}Dipartimento di Fisica, Università di Perugia, I-06100 Perugia, Italy^{57a}INFN Sezione di Pisa, I-56127 Pisa, Italy^{57b}Dipartimento di Fisica, Università di Pisa, I-56127 Pisa, Italy^{57c}Scuola Normale Superiore di Pisa, I-56127 Pisa, Italy⁵⁸Princeton University, Princeton, New Jersey 08544, USA^{59a}INFN Sezione di Roma, I-00185 Roma, Italy^{59b}Dipartimento di Fisica, Università di Roma La Sapienza, I-00185 Roma, Italy⁶⁰Universität Rostock, D-18051 Rostock, Germany⁶¹Rutherford Appleton Laboratory, Chilton, Didcot, Oxon OX11 0QX, United Kingdom⁶²CEA, Irfu, SPP, Centre de Saclay, F-91191 Gif-sur-Yvette, France⁶³SLAC National Accelerator Laboratory, Stanford, California 94309, USA⁶⁴University of South Carolina, Columbia, South Carolina 29208, USA⁶⁵Southern Methodist University, Dallas, Texas 75275, USA⁶⁶Stanford University, Stanford, California 94305-4060, USA⁶⁷State University of New York, Albany, New York 12222, USA⁶⁸School of Physics and Astronomy, Tel Aviv University, Tel Aviv 69978, Israel⁶⁹University of Tennessee, Knoxville, Tennessee 37996, USA⁷⁰University of Texas at Austin, Austin, Texas 78712, USA⁷¹University of Texas at Dallas, Richardson, Texas 75083, USA^{72a}INFN Sezione di Torino, I-10125 Torino, Italy^{72b}Dipartimento di Fisica Sperimentale, Università di Torino, I-10125 Torino, Italy^{73a}INFN Sezione di Trieste, I-34127 Trieste, Italy^{73b}Dipartimento di Fisica, Università di Trieste, I-34127 Trieste, Italy⁷⁴IFIC, Universitat de Valencia-CSIC, E-46071 Valencia, Spain⁷⁵University of Victoria, Victoria, British Columbia, Canada V8W 3P6⁷⁶Department of Physics, University of Warwick, Coventry CV4 7AL, United Kingdom⁷⁷University of Wisconsin, Madison, Wisconsin 53706, USA

(Received 19 June 2012; published 6 March 2013)

We present improved measurements of CP -violation parameters in the decays $B^0 \rightarrow \pi^+ \pi^-$, $B^0 \rightarrow K^+ \pi^-$, and $B^0 \rightarrow \pi^0 \pi^0$, and of the branching fractions for $B^0 \rightarrow \pi^0 \pi^0$ and $B^0 \rightarrow K^0 \pi^0$. The results are obtained with the full data set collected at the $\Upsilon(4S)$ resonance by the $BABAR$ experiment at the PEP-II asymmetric-energy B factory at the SLAC National Accelerator Laboratory, corresponding to $(467 \pm 5) \times 10^6$ $B\bar{B}$ pairs. We find the CP -violation parameter values and branching fractions: $S_{\pi^+ \pi^-} = -0.68 \pm 0.10 \pm 0.03$, $C_{\pi^+ \pi^-} = -0.25 \pm 0.08 \pm 0.02$, $\mathcal{A}_{K^+ \pi^+} = -0.107 \pm 0.016_{-0.004}^{+0.006}$, $C_{\pi^0 \pi^0} = -0.43 \pm 0.26 \pm 0.05$, $\mathcal{B}(B^0 \rightarrow \pi^0 \pi^0) = (1.83 \pm 0.21 \pm 0.13) \times 10^{-6}$, $\mathcal{B}(B^0 \rightarrow K^0 \pi^0) = (10.1 \pm 0.6 \pm 0.4) \times 10^{-6}$, where in each case, the first uncertainties are statistical and the second are systematic. We observe CP violation with a significance of 6.7 standard deviations for $B^0 \rightarrow \pi^+ \pi^-$ and 6.1 standard deviations for $B^0 \rightarrow K^+ \pi^-$, including systematic uncertainties. Constraints on the unitarity triangle angle α are determined from the isospin relations among the $B \rightarrow \pi\pi$ rates and asymmetries. Considering only the solution preferred by the Standard Model, we find α to be in the range $[71^\circ, 109^\circ]$ at the 68% confidence level.

DOI: [10.1103/PhysRevD.87.052009](https://doi.org/10.1103/PhysRevD.87.052009)

PACS numbers: 13.66.Bc, 13.25.Hw, 13.25.Jx, 14.40.Nd

*Present address: University of Tabuk, Tabuk 71491, Saudi Arabia.

†Also at Università di Perugia, Dipartimento di Fisica, Perugia, Italy.

‡Present address: University of Huddersfield, Huddersfield HD1 3DH, United Kingdom.

§Deceased.

||Present address: University of South Alabama, Mobile, Alabama 36688, USA.

¶Also at Università di Sassari, Sassari, Italy.

I. INTRODUCTION

Large CP -violating effects [1] in the B -meson system are among the most remarkable predictions of the Cabibbo-Kobayashi-Maskawa (CKM) quark-mixing model [2]. These predictions have been confirmed by the *BABAR* and Belle Collaborations, most precisely in $b \rightarrow c\bar{c}s$ decays of B^0 mesons to CP eigenstates [3,4].

Effective constraints on physics beyond the Standard Model (SM) are provided by high-precision measurements of quantities whose SM predictions are subject to only small theoretical uncertainties. Many experimental and theoretical uncertainties partially cancel in the calculation of CP -violating asymmetries. This makes CP -violation measurements a sensitive probe for effects of yet-undiscovered additional interactions and heavy particles that are introduced by extensions to the SM. All measurements of CP violation to date, including those involving the decay modes studied here [5–9], are in agreement with the indirect predictions from global SM fits [10,11], which are based on measurements of the magnitudes of the elements V_{ij} of the CKM quark-mixing matrix. This strongly constrains [12] the flavor structure of SM extensions.

The CKM-matrix unitarity triangle angle $\alpha \equiv \arg[-V_{td}V_{tb}^*/V_{ud}V_{ub}^*]$ is measured through interference between two decay amplitudes, where one amplitude involves B^0 - \bar{B}^0 mixing. Multiple measurements of α , with different decays, further test the consistency of the CKM model. The time-dependent asymmetry in $B^0 \rightarrow \pi^+\pi^-$ decays is proportional to $\sin 2\alpha$ in the limit that only the $b \rightarrow u$ (“tree”) quark-level amplitude contributes to this decay. In the presence of $b \rightarrow d$ (“penguin”) amplitudes, the time-dependent asymmetry in $B^0 \rightarrow \pi^+\pi^-$ is modified to

$$a(\Delta t) = \frac{|\bar{A}(\Delta t)^2 - |A(\Delta t)|^2}{|\bar{A}(\Delta t)^2 + |A(\Delta t)|^2} \\ = S_{\pi^+\pi^-} \sin(\Delta m_d \Delta t) - C_{\pi^+\pi^-} \cos(\Delta m_d \Delta t), \quad (1)$$

where Δt is the difference between the proper decay times of the B meson that undergoes the $B \rightarrow \pi^+\pi^-$ decay (the signal B) and the other B meson in the event (the tag B), Δm_d is the B^0 - \bar{B}^0 mixing frequency, A is the $B^0 \rightarrow \pi^+\pi^-$ decay amplitude, \bar{A} is the CP -conjugate amplitude, and

$$C_{\pi^+\pi^-} = \frac{|A|^2 - |\bar{A}|^2}{|A|^2 + |\bar{A}|^2}, \quad (2) \\ S_{\pi^+\pi^-} = \sqrt{1 - C_{\pi^+\pi^-}^2} \sin(2\alpha - 2\Delta\alpha_{\pi\pi}).$$

Both the direct CP asymmetry $C_{\pi^+\pi^-}$ and the phase $\Delta\alpha_{\pi\pi}$ may differ from zero due to the penguin contribution to the decay amplitudes.

The magnitude and relative phase of the penguin contribution to the asymmetry $S_{\pi^+\pi^-}$ may be determined with an analysis of isospin relations between the $B \rightarrow \pi\pi$ decay amplitudes [13]. The amplitudes A^{ij} of the $B \rightarrow \pi^i\pi^j$ decays and \bar{A}^{ij} of the $\bar{B} \rightarrow \pi^i\pi^j$ decays satisfy the relations

$$A^{+0} = \frac{1}{\sqrt{2}}A^{+-} + A^{00}, \quad \bar{A}^{-0} = \frac{1}{\sqrt{2}}\bar{A}^{+-} + \bar{A}^{00}. \quad (3)$$

The shapes of the triangles corresponding to these isospin relations are determined from measurements of the branching fractions and time-integrated CP asymmetries for each of the $B \rightarrow \pi\pi$ decays. Gluonic penguin amplitudes do not contribute to the $\Delta I = 3/2$ decay $B^\pm \rightarrow \pi^\pm\pi^0$. Therefore, neglecting electroweak (EW) penguin amplitudes, the amplitudes A^{+0} and \bar{A}^{-0} are equal. From the different shapes of the triangles for the B and \bar{B} decay amplitudes, a constraint on $\Delta\alpha_{\pi\pi}$ can be determined to within a fourfold ambiguity.

The phenomenology of the $B \rightarrow \pi\pi$ system has been thoroughly studied in a number of theoretical frameworks and models [14]. Predictions for the relative size and phase of the penguin contribution vary considerably. Therefore, increasingly precise measurements will help distinguish among different theoretical approaches and add to our understanding of hadronic B decays.

The measured rates and direct CP -violating asymmetries in $B \rightarrow K\pi$ decays [6,7,9,15–18] reveal puzzling features that could indicate significant contributions from EW penguin amplitudes [19,20]. Various methods have been proposed for isolating the SM contribution to this process in order to test for signs of new physics. This includes sum rules derived from U -spin symmetry, which relate the rates and asymmetries for the decays of charged or neutral B mesons to $K^+\pi^-$, $K^+\pi^0$, $K^0\pi^0$, and $K^0\pi^+$ [21,22], and $SU(3)$ symmetry used to make predictions for the $K\pi$ system based on hadronic parameters extracted from the $\pi\pi$ system [19].

This article is organized as follows. The *BABAR* detector and the data used in these measurements are described in Sec. II. In Sec. III we outline the analysis method, including the event selection and the fits used to extract the parameters of interest. The results of the data analysis are given in Sec. IV. The extraction of α and $\Delta\alpha_{\pi\pi}$ is described in Sec. V, and we summarize in Sec. VI.

II. THE *BABAR* DETECTOR AND DATA SET

In the *BABAR* detector [23], charged particles are detected and their momenta are measured by the combination of a five-layer double-sided silicon vertex tracker (SVT) and a 40-layer drift chamber (DCH) that covers 92% of the solid angle in the $Y(4S)$ center-of-mass (c.m.) frame, both operating in a 1.5-T uniform magnetic field. Discrimination between charged pions, kaons, and protons is obtained from ionization (dE/dx) measurements in the DCH and from an internally reflecting ring-imaging Cherenkov detector (DIRC), which covers 84% of the c.m. solid angle in the central region of the *BABAR* detector and has a 91% reconstruction efficiency for pions and kaons with momenta above 1.5 GeV/ c . Photons and electrons are identified and their energies are measured with

an electromagnetic calorimeter (EMC) consisting of 6580 CsI(Tl) crystals. The photon energy resolution is $\sigma_E/E = \{2.3/E(\text{GeV})^{1/4} \oplus 1.4\}\%$, and the photon angular resolution relative to the interaction point is $\sigma_\theta = 4.16/\sqrt{E(\text{GeV})}$ mrad [24].

The data used in this analysis were collected during the period 1999–2007 with the *BABAR* detector at the PEP-II asymmetric-energy B -meson factory at the SLAC National Accelerator Laboratory. A total of $(467 \pm 5) \times 10^6$ $B\bar{B}$ pairs were used. Relative to previous *BABAR* measurements [5–7], roughly 22% more $B\bar{B}$ pairs have been added to the analyzed data set, and improvements have been introduced to the analysis technique, boosting the signal significance. These improvements include better reconstruction of charged-particle tracks, improved hadron identification and flavor-tagging algorithms, and optimal selection of tracks and calorimeter clusters for calculation of event-shape variables.

Samples of Monte Carlo (MC) simulated events are analyzed with the same reconstruction and analysis procedures as used for the data, following a Geant4-based [25] detailed detector simulation [23]. The MC samples include $e^+e^- \rightarrow q\bar{q}$ continuum background events generated with JETSET [26] and $Y(4S) \rightarrow B\bar{B}$ decays generated with EvtGen [27] and JETSET, including both signal and background B -meson decays.

III. EVENT SELECTION AND ANALYSIS METHOD

Many elements of the measurements discussed in this paper are common to the decay modes [28] $B^0 \rightarrow h^+h'^-$ (where $h, h' = \pi$ or K), $B^0 \rightarrow \pi^0\pi^0$, and $B^0 \rightarrow K_S^0\pi^0$. The signal B -meson candidates (B_{rec}) are formed by combining two particles, each of which is a charged-particle track, a π^0 candidate, or a K_S^0 candidate. The event selection differs for each mode and is described below.

The number of B decays and the corresponding CP asymmetries are determined with extended unbinned maximum likelihood (ML) fits to variables described below. The likelihood is given by the expression

$$\mathcal{L} = \exp\left(-\sum_i^M n_i\right) \prod_j^N \left[\sum_i^M n_i \mathcal{P}_i(\vec{x}_j; \vec{\alpha}_i)\right], \quad (4)$$

where N is the number of events, the sums are over the event categories M , n_i is the event yield for each category as described below, and the probability-density function (PDF) \mathcal{P}_i describes the distribution of the variables \vec{x}_j in terms of parameters $\vec{\alpha}_i$. The PDF functional forms are discussed in Secs. III C and III D.

A. Track and K_S^0 selection

In the $B^0 \rightarrow h^+h'^-$ mode, we require charged-particle tracks to have at least 12 DCH hits and to lie in the

polar-angle region $0.35 < \theta < 2.40$ with respect to the beam direction. The track impact parameter relative to the e^+e^- collision axis must be smaller than 1.5 cm in the plane perpendicular to the beam axis and 2.5 cm in the direction along the axis.

In order for DIRC information to be used for particle identification, we require that each track have its associated Cherenkov angle (θ_C) measured with at least six Cherenkov photons, where the value of θ_C is required to be within 4.0 standard deviations (σ) of either the pion or kaon hypothesis. This removes candidates containing a high-momentum proton. Tracks from electrons are removed based primarily on a comparison of the track momentum and the associated energy deposition in the EMC, with additional information provided by DCH dE/dx and DIRC θ_C measurements.

The ionization energy loss in the DCH is used either in combination with DIRC information or alone. This leads to a 35% increase in the $B^0 \rightarrow h^+h'^-$ reconstruction efficiency relative to the use of only tracks with good DIRC information. A detailed DCH dE/dx calibration developed for the $B^0 \rightarrow h^+h'^-$ analysis takes into account variations in the mean and resolution of dE/dx measurement values with respect to changes in the DCH running conditions over time, as well as the track's charge, polar and azimuthal angles, and number of ionization samples. The calibration is performed with large high-purity samples (with more than 10^6 events) of protons from $\Lambda \rightarrow p\pi^-$, pions and kaons from $D^{*+} \rightarrow D^0\pi^+(D^0 \rightarrow K^-\pi^+)$, and $K_S^0 \rightarrow \pi^+\pi^-$ decays that occur in the vicinity of the interaction region.

Candidates for the decay $K_S^0 \rightarrow \pi^+\pi^-$ are reconstructed from pairs of oppositely charged tracks. The two-track combinations are required to form a vertex with a χ^2 probability greater than 0.001 and a $\pi^+\pi^-$ invariant mass within $11.2 \text{ MeV}/c^2$, corresponding to 3.7σ , of the nominal K_S^0 mass [29].

B. π^0 selection

We form $\pi^0 \rightarrow \gamma\gamma$ candidates from pairs of clusters in the EMC that are isolated from any charged track. Clusters are required to have a lateral profile of energy deposition consistent with that of a photon and to have an energy $E_\gamma > 30 \text{ MeV}$ for $B^0 \rightarrow \pi^0\pi^0$ and $E_\gamma > 50 \text{ MeV}$ for $B^0 \rightarrow K_S^0\pi^0$. We require π^0 candidates to lie in the invariant-mass range $110 < m_{\gamma\gamma} < 160 \text{ MeV}/c^2$.

For the $B^0 \rightarrow \pi^0\pi^0$ mode, we also use π^0 candidates from a single EMC cluster containing two adjacent photons (a merged π^0), or one EMC cluster and two tracks from a photon conversion to an e^+e^- pair inside the detector. To reduce the background from random photon combinations, the angle θ_γ between the photon momentum vector in the π^0 rest frame and the π^0 momentum vector in the laboratory frame is required to satisfy $|\cos \theta_\gamma| < 0.95$. The π^0 candidates are fitted

kinematically with their mass constrained to the nominal π^0 mass [29].

Photon conversions are selected from pairs of oppositely charged electron-candidate tracks with an invariant mass below $30 \text{ MeV}/c^2$ whose combined momentum vector points away from the beam spot. The conversion point is required to lie within detector material layers. Converted photons are combined with photons from single EMC clusters to form π^0 candidates.

Single EMC clusters containing two photons are selected with the transverse second moment, $S = \sum_i E_i \times (\Delta\alpha_i)^2/E$, where E_i is the energy in each CsI(Tl) crystal and $\Delta\alpha_i$ is the angle between the cluster centroid and the crystal. The second moment is used to distinguish merged π^0 candidates from both single photons and neutral hadrons.

C. $B^0 \rightarrow \pi^+ \pi^-$, $B^0 \rightarrow K^+ \pi^-$, and $B^0 \rightarrow \pi^0 \pi^0$

Two kinematic variables are used in the $B^0 \rightarrow h^+ h'^-$ and $B^0 \rightarrow \pi^0 \pi^0$ analyses to separate B -meson decays from the large $e^+ e^- \rightarrow q\bar{q}$ ($q = u, d, s, c$) combinatoric background [23]. One variable is the beam-energy-substituted mass $m_{\text{ES}} = \sqrt{(s/2 + \mathbf{p}_i \cdot \mathbf{p}_B)^2/E_i^2 - \mathbf{p}_B^2}$, where \sqrt{s} is the total $e^+ e^-$ c.m. energy, (E_i, \mathbf{p}_i) is the four-momentum of the initial $e^+ e^-$ system in the laboratory frame, and \mathbf{p}_B is the laboratory momentum of the B candidate. The second variable is $\Delta E = E_B^* - \sqrt{s}/2$, where E_B^* is the energy of the B candidate in the c.m. frame.

To further separate B decays from the $q\bar{q}$ background, we use two additional topological variables that take advantage of the two-jet nature of $q\bar{q}$ events and the isotropic particle distribution of $e^+ e^- \rightarrow B\bar{B}$ events. The first variable is the absolute value of the cosine of the angle θ_S between the sphericity axis [30] of the decay products of the B candidate and the sphericity axis of the remaining tracks and neutral clusters in the event, computed in the c.m. frame. The distribution of this variable peaks at 1 for the jetlike $q\bar{q}$ events and is uniform for B decays. We require $|\cos \theta_S| < 0.91$ for $B^0 \rightarrow h^+ h'^-$ and $|\cos \theta_S| < 0.7$ for $B^0 \rightarrow \pi^0 \pi^0$, where a tighter requirement is needed due to the higher background. For the $B^0 \rightarrow h^+ h'^-$ mode, we remove a small remaining background from $e^+ e^- \rightarrow \tau^+ \tau^-$ events by further requiring that the normalized second Fox-Wolfram moment [31] satisfy $R_2 < 0.7$.

To improve the discrimination against $q\bar{q}$ events, a Fisher discriminant \mathcal{F} is formed as a linear combination of the sums $L_0^T \equiv \sum_i |\mathbf{p}_i^*|$ and $L_2^T \equiv \sum_i |\mathbf{p}_i^*| \cos^2 \theta_i^*$, where \mathbf{p}_i^* are the momenta and θ_i^* are the angles with respect to the thrust axis [32] of the B candidate, both in the c.m. frame, of all tracks and clusters not used to reconstruct the signal B -meson candidate. The \mathcal{F} variable takes advantage of the fact that much of the momentum flow in $q\bar{q}$ events is along the thrust axis. In the case of $B^0 \rightarrow \pi^0 \pi^0$, we improve the sensitivity to signal events by combining \mathcal{F} with three other event-shape variables in a neural network. The

first variables is $|\cos \theta_S|$, described above. The second is $|\cos \theta_B^*|$, where θ_B^* is the angle between the momentum vector of the signal B and the beam axis. The $|\cos \theta_B^*|$ distribution of $q\bar{q}$ events is uniform, while that of signal events is proportional to $\sin^2 \theta_B^*$. The third variable is $|\cos \theta_T^*|$, where θ_T^* is the angle between the thrust axis of the signal B -meson's daughters and the beam axis. Both θ_B^* and θ_T^* are calculated in the c.m. frame. The characteristics of the $|\cos \theta_T^*|$ distributions are similar to those of $|\cos \theta_S|$.

I. $B^0 \rightarrow \pi^+ \pi^-$ and $B^0 \rightarrow K^+ \pi^-$

We reconstruct the candidate decays $B_{\text{rec}} \rightarrow h^+ h'^-$ from pairs of oppositely charged tracks that are consistent with originating from a common decay point with a χ^2 probability of at least 0.001. The remaining particles are examined to infer whether the other B meson in the event (B_{tag}) decayed as a B^0 or \bar{B}^0 (flavor tag). We perform an unbinned extended ML fit to separate $B^0 \rightarrow \pi^+ \pi^-$ and $B^0 \rightarrow K^+ \pi^-$ decays and determine simultaneously their CP -violating asymmetries $S_{\pi^+ \pi^-}$, $C_{\pi^+ \pi^-}$, and

$$\mathcal{A}_{K^+ \pi^-} = \frac{\mathcal{B}(B \rightarrow K^- \pi^+) - \mathcal{B}(B \rightarrow K^+ \pi^-)}{\mathcal{B}(B \rightarrow K^- \pi^+) + \mathcal{B}(B \rightarrow K^+ \pi^-)}, \quad (5)$$

as well as the signal and background yields and PDF parameters. The fit uses θ_C , dE/dx , ΔE , m_{ES} , \mathcal{F} , B_{tag} flavor, and Δt information.

The value of ΔE is calculated assuming that both tracks are charged pions. The $B^0 \rightarrow \pi^+ \pi^-$ signal is described by a Gaussian distribution for ΔE , with a resolution of 29 MeV. For each kaon in the final state, the ΔE peak position is shifted from zero by an amount that depends on the kaon momentum, with an average shift of -45 MeV. We require $|\Delta E| < 0.150$ GeV. The wide range in ΔE allows us to separate B^0 decays to the four final states $\pi^+ \pi^-$, $K^+ \pi^-$, $\pi^+ K^-$, and $K^+ K^-$ in a single fit. The analysis is not optimized for measuring the $K^+ K^-$ final state, which is treated as background. The m_{ES} resolution is $2.6 \text{ MeV}/c^2$. We require $m_{\text{ES}} > 5.20 \text{ GeV}/c^2$, with events in the large range below the signal peak allowing the fit to effectively determine the background shape parameters.

We construct θ_C PDFs for the pion and kaon hypotheses, and dE/dx PDFs for the pion, kaon, and proton hypotheses, separately for each charge. The K - π separations provided by θ_C and dE/dx are complementary: for θ_C , the separation varies from 2.5σ at $4.5 \text{ GeV}/c$ to 13σ at $1.5 \text{ GeV}/c$, while for dE/dx it varies from less than 1.0σ at $1.5 \text{ GeV}/c$ to 1.9σ at $4.5 \text{ GeV}/c$ (Fig. 1). For more details, see Ref. [5].

We use a multivariate technique [33] to determine the flavor of the B_{tag} . Separate neural networks are trained to identify leptons from B decays, kaons from D decays, and soft pions from D^* decays. Events are assigned to one of seven mutually exclusive tagging categories (one category being untagged events) based on the estimated average

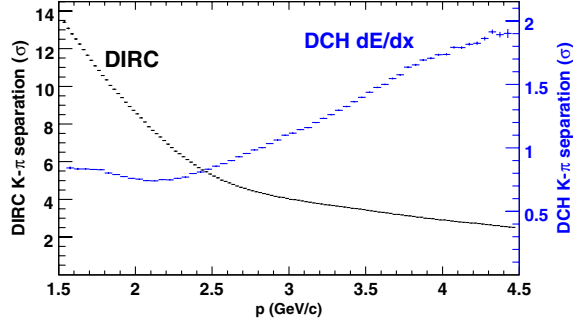


FIG. 1 (color online). The average expected K - π separation, in units of uncertainty, provided by the DIRC angle θ_C and DCH dE/dx for kaons and pions from $B^0 \rightarrow K^+ \pi^-$ decays in the laboratory-frame polar angle range $0.35 < \theta < 2.40$, as a function of laboratory-frame momentum.

mistag probability and the source of the tagging information. The quality of tagging is expressed in terms of the effective efficiency $Q = \sum_k \epsilon_k (1 - 2w_k)^2$, where ϵ_k and w_k are the efficiencies and mistag probabilities, respectively, for events tagged in category k . The difference between the mistag probabilities for B^0 and \bar{B}^0 mesons is given by $\Delta w = w_{B^0} - w_{\bar{B}^0}$. Table I summarizes the tagging performance measured in a large data sample of fully reconstructed neutral B_{flav} decays to $D^{(*)-}(\pi^+, \rho^+, a_1^+)$ [34].

The time difference $\Delta t = \Delta z / \beta \gamma c$ is obtained from the known boost of the $e^+ e^-$ system ($\beta \gamma = 0.56$) and the measured distance Δz along the beam (z) axis between the B_{rec} and B_{tag} decay vertices. A description of the inclusive reconstruction of the B_{tag} vertex is given in Ref. [35]. We require $|\Delta t| < 20$ ps and $\sigma_{\Delta t} < 2.5$ ps, where $\sigma_{\Delta t}$ is the uncertainty on Δt estimated separately for each event. The signal Δt PDF for $B^0 \rightarrow \pi^+ \pi^-$ is given by

$$f_k^\pm(\Delta t_{\text{meas}}) = \frac{e^{-|\Delta t|/\tau}}{4\tau} \{ (1 \mp \Delta w) \pm (1 - 2w_k) \times [S_{\pi^+ \pi^-} \sin(\Delta m_d \Delta t) - C_{\pi^+ \pi^-} \cos(\Delta m_d \Delta t)] \} \otimes R(\Delta t_{\text{meas}} - \Delta t), \quad (6)$$

TABLE I. Average tagging efficiency ϵ , average mistag fraction w , mistag fraction difference $\Delta w = w(B^0) - w(\bar{B}^0)$, and effective tagging efficiency Q for signal events in each tagging category (except the untagged category).

Category	ϵ (%)	w (%)	Δw (%)	Q (%)
LEPTON	8.96 ± 0.07	2.9 ± 0.3	0.2 ± 0.5	7.95 ± 0.11
KAON I	10.81 ± 0.07	5.3 ± 0.3	0.0 ± 0.6	8.64 ± 0.14
KAON II	17.18 ± 0.09	14.5 ± 0.3	0.4 ± 0.6	8.64 ± 0.17
KAON PION	13.67 ± 0.08	23.3 ± 0.4	-0.6 ± 0.7	3.91 ± 0.12
PION	14.19 ± 0.08	32.6 ± 0.4	5.1 ± 0.7	1.73 ± 0.09
OTHER	9.55 ± 0.07	41.5 ± 0.5	3.8 ± 0.8	0.28 ± 0.04
Total				31.1 ± 0.3

where f_k^+ (f_k^-) indicates a B^0 (\bar{B}^0) flavor tag and the index k indicates the tagging category. The resolution function $R(\Delta t_{\text{meas}} - \Delta t)$ for signal candidates is a sum of three Gaussian functions, identical to the one described in Ref. [35], with parameters determined from a fit to the B_{flav} sample, which includes events in all seven tagging categories. The background Δt distribution is modeled as the sum of three Gaussians, with parameters, common for all tagging categories, determined simultaneously with the CP -violation parameters in the ML fit to the $B_{\text{rec}} \rightarrow h^+ h'^-$ sample.

The ML fit PDF includes 28 components. Of these, 24 components correspond to B^0 signal decays and background events with the final states $\pi^+ \pi^-$, $K^+ \pi^-$, $K^- \pi^+$, and $K^+ K^-$, where either the positively charged track, the negatively charged track, or both have good DIRC information ($2 \times 4 \times 3 = 24$ components). Four additional components correspond to $p \pi^-$, $p K^-$, $\pi^+ \bar{p}$, and $K^+ \bar{p}$ background events, where the (anti)proton has no DIRC information. The $K^\pm \pi^\mp$ event yields $n_{K^\pm \pi^\mp}$ are parametrized in terms of the asymmetry $\mathcal{A}_{K^\pm \pi^\mp}^{\text{raw}}$ and average yield $n_{K\pi}$ as $n_{K^\pm \pi^\mp} = n_{K\pi} (1 \mp \mathcal{A}_{K^\pm \pi^\mp}^{\text{raw}}) / 2$. All other event yields are products of the fraction of events in each tagging category taken from B_{flav} events, and the total event yield. The background PDFs are a threshold function [36] for m_{ES} and a second-order polynomial for ΔE . The \mathcal{F} PDF is a sum of two asymmetric Gaussians for both signal and background. We use large samples of simulated B decays to investigate the effects of backgrounds from other B decays on the determination of the CP -violating asymmetries in $B^0 \rightarrow \pi^+ \pi^-$ and $B^0 \rightarrow K^+ \pi^-$, and find them to be negligible.

2. $B^0 \rightarrow \pi^0 \pi^0$

$B^0 \rightarrow \pi^0 \pi^0$ events are identified with a ML fit to the variables m_{ES} , ΔE , and the output NN of the event-shape neural network. We require $m_{\text{ES}} > 5.20$ GeV/ c^2 and $|\Delta E| < 0.2$ GeV. Since tails in the EMC response produce a correlation between m_{ES} and ΔE , a two-dimensional binned PDF derived from the signal MC sample is used to describe signal PDF. The NN distribution is divided into ten bins (with each bin approximately equally populated by signal events) and described by a nine-bin step-function PDF with values taken from the MC and fixed in the fit. B_{flav} data are used to verify that the MC accurately reproduces the NN distribution. The $q\bar{q}$ background PDFs are a threshold function [36] for m_{ES} , a second-order polynomial for ΔE , and a parametric step function for NN . For $q\bar{q}$ events, NN is not distributed uniformly across the bins but rises sharply toward the highest bins. We see a small correlation of 2.5% between the shape parameter of the m_{ES} threshold function and the NN bin number, and this relation is taken into account in the fit. All $q\bar{q}$ background PDF-parameter values are determined by the ML fit.

The decays $B^+ \rightarrow \rho^+ \pi^0$ and $B^0 \rightarrow K_S^0 \pi^0 (K_S^0 \rightarrow \pi^0 \pi^0)$ add 71 ± 10 background events to $B^0 \rightarrow \pi^0 \pi^0$ and are included as an additional component in the ML fit. We model these B -decay background events with a two-dimensional binned PDF in m_{ES} and ΔE , and with a step function for NN . The shapes of these PDFs are taken from MC simulation, and their event yields and asymmetries are fixed in the fit and are later varied to evaluate systematic uncertainties.

The time-integrated CP asymmetry is measured by the B -flavor tagging algorithm described above. The fraction of events in each tagging category is constrained to the corresponding fraction determined from MC simulation. The PDF event yields for the $B^0 \rightarrow \pi^0 \pi^0$ signal are given by the expression

$$n_{\pi^0 \pi^0, k} = \frac{1}{2} f_k N_{\pi^0 \pi^0} [1 - s_j (1 - 2\chi)(1 - 2w_k) C_{\pi^0 \pi^0}], \quad (7)$$

where f_k is the fraction of events in tagging category k , $N_{\pi^0 \pi^0}$ is the number of $B^0 \rightarrow \pi^0 \pi^0$ candidate decays, χ is the time-integrated B^0 mixing probability [29], $s_j = +1(-1)$ when the B_{tag} is a B^0 (\bar{B}^0), and

$$C_{\pi^0 \pi^0} = \frac{|A^{00}|^2 - |\bar{A}^{00}|^2}{|A^{00}|^2 + |\bar{A}^{00}|^2} \quad (8)$$

is the direct CP asymmetry in $B^0 \rightarrow \pi^0 \pi^0$.

D. $B^0 \rightarrow K_S^0 \pi^0$

CP -violation parameters for $B^0 \rightarrow K_S^0 \pi^0$ have been reported in Ref. [4]. Here we describe the measurement of the branching fraction for this mode.

For each $B^0 \rightarrow K_S^0 \pi^0$ candidate, two independent kinematic variables are computed. The first variable is the invariant mass m_B of the B_{rec} . The second variable is the invariant (missing) mass m_{miss} of the B_{tag} , computed from the magnitude of the difference between the four-momentum of the initial $e^+ e^-$ system and that of the B_{rec} , after applying a B^0 -mass constraint to the B_{rec} [37]. For signal decays, m_B and m_{miss} peak near the B^0 mass with resolutions of about 36 and 5.3 MeV/ c^2 , respectively. Since the linear correlation coefficient between m_B and m_{miss} vanishes, these variables yield better separation of signal from background than m_{ES} and ΔE . Both the m_B and m_{miss} distributions exhibit a low-side tail due to leakage of energy out of the EMC. We select candidates within the ranges $5.13 < m_B < 5.43$ GeV/ c^2 and $5.11 < m_{\text{miss}} < 5.31$ GeV/ c^2 , which include a signal peak and a ‘‘sideband’’ region for background characterization. In events with more than one reconstructed candidate (0.8% of the total), we select the candidate with the smallest $\chi^2 = \sum_{i=\pi^0, K_S^0} (m_i - m_i^l)^2 / \sigma_{m_i}^2$, where m_i (m_i^l) is the measured (nominal) mass and σ_{m_i} is the estimated uncertainty on the measured mass of particle i .

We exploit topological observables computed in the c.m. frame to discriminate jetlike $e^+ e^- \rightarrow q\bar{q}$ events from the nearly spherical $B\bar{B}$ events. In order to reduce the number of background events, we require $L_2/L_0 < 0.55$, where $L_j \equiv \sum_i |\mathbf{p}_i^*| \cos^j \theta_i^*$ and θ_i^* are computed with respect to the sphericity axis [30] of the B_{rec} candidate. Taking advantage of the fact that signal events follow a $1 - \cos^2 \theta_B^*$ distribution while the background is flat, we select events with $|\cos \theta_B^*| < 0.9$. Using a full detector simulation, we estimate that our selection retains $34.2\% \pm 1.2\%$ of the signal events, where the uncertainty includes both statistical and systematic contributions. The selected sample of $B^0 \rightarrow K_S^0 \pi^0$ candidates is dominated by random $K_S^0 \pi^0$ combinations from $e^+ e^- \rightarrow q\bar{q}$ events. Using large samples of simulated $B\bar{B}$ events, we find that backgrounds from other B -meson decays are small, of order 0.1%. Therefore, this type of background is not included in the fit described below, and this is accounted for in the evaluation of systematic uncertainties (see Sec. IV C).

We extract the signal yield from an extended unbinned ML fit to m_B , m_{miss} , L_2/L_0 , $\cos \theta_B^*$, the flavor tag, and the decay time and its error. The use of tagging and decay-time information in the ML fit further improves discrimination between signal and background. Since in the $B^0 \rightarrow K_S^0 \pi^0$ decay no charged particles originate from the decay vertex, we compute the decay point of the B_{rec} using the K_S^0 trajectory obtained from the reconstructed K_S^0 decay vertex and momentum vector, and the average $e^+ e^-$ interaction point [38]. We have verified that all correlations between the fit variables are negligible and so construct the likelihood function as a product of one-dimensional PDFs. Residual correlations are taken into account in the systematic uncertainty, as explained below.

The PDFs for signal events are parametrized based on a large sample of fully reconstructed B decays in data and from simulated events. For background PDFs, we take the functional form from the background-dominated sideband regions in the data. The likelihood function is

$$\begin{aligned} \mathcal{L}(S_{K_S^0 \pi^0}, C_{K_S^0 \pi^0}, N_S, N_B, f_S^g, f_B^g, \vec{\alpha}) \\ = \frac{e^{-(N_S + N_B)}}{N!} \prod_{i \in g} [N_S f_S^g \epsilon_S^c \mathcal{P}_S(\vec{x}_i, \vec{y}_i; S_{K_S^0 \pi^0}, C_{K_S^0 \pi^0}) \\ + N_B f_B^g \epsilon_B^c \mathcal{P}_B(\vec{x}_i, \vec{y}_i; \vec{\alpha})] \prod_{i \in b} [N_S f_S^b \epsilon_S^c \mathcal{P}_S^l(\vec{x}_i; C_{K_S^0 \pi^0}) \\ + N_B f_B^b \epsilon_B^c \mathcal{P}_B^l(\vec{x}_i; \vec{\alpha})], \end{aligned} \quad (9)$$

where the N selected events are partitioned into two subsets: the index $i \in g$ indicates events that have Δt information, while $i \in b$ events do not have Δt information. Here, f_S^g (f_B^g) is the fraction of signal (background) events that are in the subset g , and $f_S^b = 1 - f_S^g$ ($f_B^b = 1 - f_B^g$) are the corresponding signal (background) fractions in the subset b . The parameter N_S (N_B) is the number of signal (background) events. The probabilities \mathcal{P}_S and \mathcal{P}_B

TABLE II. Results for the $B^0 \rightarrow h^+ h'^-$ decay modes. Uncertainties on the signal yields N_{sig} are statistical. For the CP -violation parameters, the first uncertainties are statistical, and the second are systematic.

Mode	N_{sig}	CP -violation parameters
$B^0 \rightarrow \pi^+ \pi^-$	1394 ± 54	$S_{\pi^+ \pi^-} = -0.68 \pm 0.10 \pm 0.03$ $C_{\pi^+ \pi^-} = -0.25 \pm 0.08 \pm 0.02$
$B^0 \rightarrow K^+ \pi^-$	5410 ± 90	$\mathcal{A}_{K^+ \pi^-} = -0.107 \pm 0.016^{+0.006}_{-0.004}$
$B^0 \rightarrow K^+ K^-$	7 ± 17	

are products of PDFs for the signal and background hypotheses evaluated for the measurements $\vec{x}_i = \{m_B, m_{\text{miss}}, L_2/L_0, \cos \theta_B^*, \text{flavor tag, tagging category}\}$ and $\vec{y}_i = \{\Delta t, \sigma_{\Delta t}\}$. The corresponding PDFs for events without Δt information are \mathcal{P}'_S and \mathcal{P}'_B . Detailed descriptions of \mathcal{P}_S , \mathcal{P}_B , \mathcal{P}'_S , and \mathcal{P}'_B are given in Ref. [4]. The vector $\vec{\alpha}$ represents the set of parameters that define the shapes of the PDFs. Along with the CP asymmetries

$S_{K_S^0 \pi^0}$ and $C_{K_S^0 \pi^0}$, the fit extracts the yields N_S and N_B , the fraction of events f_S^g and f_B^g , and the parameters of the background PDFs.

IV. RESULTS AND SYSTEMATIC UNCERTAINTIES

A. $B^0 \rightarrow \pi^+ \pi^-$ and $B^0 \rightarrow K^+ \pi^-$ results

The event yields and CP -violation parameters are listed in Table II. The correlation coefficient between $S_{\pi^+ \pi^-}$ and $C_{\pi^+ \pi^-}$ is found to be -0.056 , and the correlation between $C_{\pi^+ \pi^-}$ and $\mathcal{A}_{K^+ \pi^-}$ is 0.019 . We show the m_{ES} , ΔE , and \mathcal{F} distribution for the $B \rightarrow \pi\pi$, $B \rightarrow K\pi$, and $q\bar{q}$ background in Fig. 2, where the $s\mathcal{P}$ Plots [39] weighting and background-subtraction technique is used to display a distribution for a particular type of event. The direct CP asymmetry in $B^0 \rightarrow K^+ \pi^-$ is apparent in the ΔE distributions, which are plotted separately for B^0 and \bar{B}^0 decays in Fig. 3. We show the distributions of Δt for $B^0 \rightarrow K^\pm \pi^\mp$ signal and background decays in Fig. 4. In Fig. 5, we show the distribution of Δt separately for $B^0 \rightarrow \pi^+ \pi^-$ events

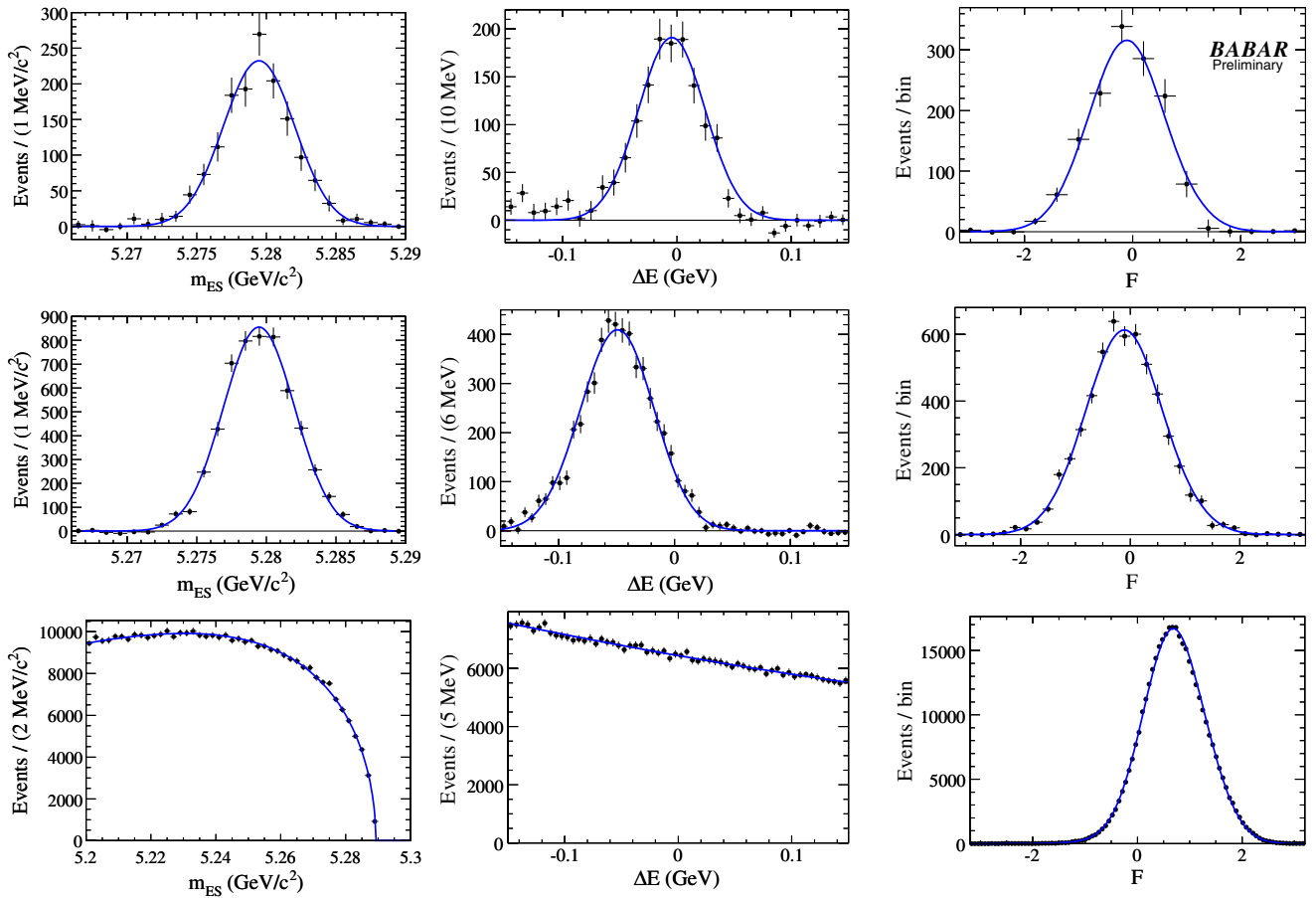


FIG. 2 (color online). $s\mathcal{P}$ Plots of the (left column) m_{ES} , (center column) ΔE , and (right column) Fisher discriminant \mathcal{F} distributions for (top row) $B^0 \rightarrow \pi^+ \pi^-$, (middle row) $B^0 \rightarrow K^+ \pi^-$, and (bottom row) $q\bar{q}$ background candidates. The points with error bars show the data, and the lines represent the PDFs used in the fit and reflect the fit result. The structure to the left of the signal ΔE peak for $B^0 \rightarrow \pi^+ \pi^-$ is consistent with the expected background from other charmless modes, which is negligible for $\Delta E > -0.10$ GeV. In the calculation of ΔE for $B^0 \rightarrow K^+ \pi^-$, the kaon candidate is assigned the pion mass.

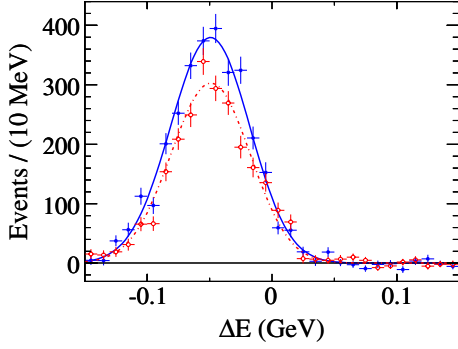


FIG. 3 (color online). \mathcal{P} lots of the ΔE distribution for signal $K^\pm \pi^\mp$ events comparing (blue solid lines, filled circles) B^0 and (red dashed lines, empty circles) \bar{B}^0 decays. The points with error bars show the data, and the lines represent the PDFs used in the fits and reflect the results of the fits.

tagged as B^0 or \bar{B}^0 , as well as the asymmetry $a(\Delta t)$ of Eq. (1). The results for $S_{\pi^+ \pi^-}$ and $C_{\pi^+ \pi^-}$ are shown in Fig. 6, along with confidence-level contours corresponding to statistical significances ranging from 1σ to 7σ . Our measurement excludes the absence of CP violation in $B^0 \rightarrow \pi^+ \pi^-$ ($S_{\pi^+ \pi^-} = 0, C_{\pi^+ \pi^-} = 0$) at a confidence level corresponding to 6.7σ , including systematic uncertainties.

Systematic uncertainties for the direct CP asymmetry $\mathcal{A}_{K^- \pi^+}$ are listed in Table III. Here, $\mathcal{A}_{K^- \pi^+}$ is the fitted value of the $K^\pm \pi^\mp$ event-yield asymmetry $\mathcal{A}_{K^- \pi^+}^{\text{raw}}$ shifted

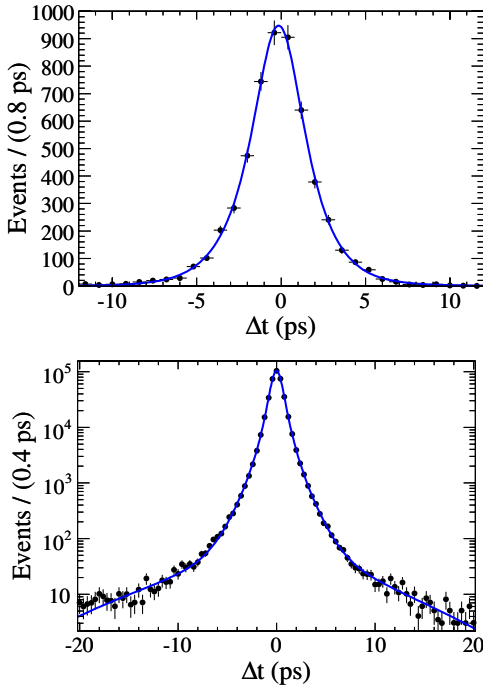


FIG. 4 (color online). \mathcal{P} lots of the Δt distribution for (top) signal $K^\pm \pi^\mp$ and (bottom) background events. The points with error bars show the data, and the lines represent the PDFs used in the fit and reflect the fit result.

by $+0.005^{+0.005}_{-0.003}$ to account for a bias that arises from the difference between the cross sections of K^+ and K^- hadronic interactions within the $BABAR$ detector. We determine this bias from the MC. The bias is independently verified with a calculation based on the known material composition of the $BABAR$ detector [23] and the cross sections and material properties tabulated in Ref. [29]. The corrected $K^\pm \pi^\mp$ event-yield asymmetry in the background where no observable CP violation is expected is $-0.005 \pm 0.004(\text{stat})^{+0.005}_{-0.003}(\text{syst})$ consistent with zero. Uncertainties on the θ_C and dE/dx distributions are obtained from the $D^0 \rightarrow K^- \pi^+$ control sample, and contribute 0.002 to the systematic uncertainty on $\mathcal{A}_{K^- \pi^+}$. An additional uncertainty of the same magnitude is obtained by adding a bifurcated-Gaussian component to the two-Gaussian θ_C PDF. We use a combination of

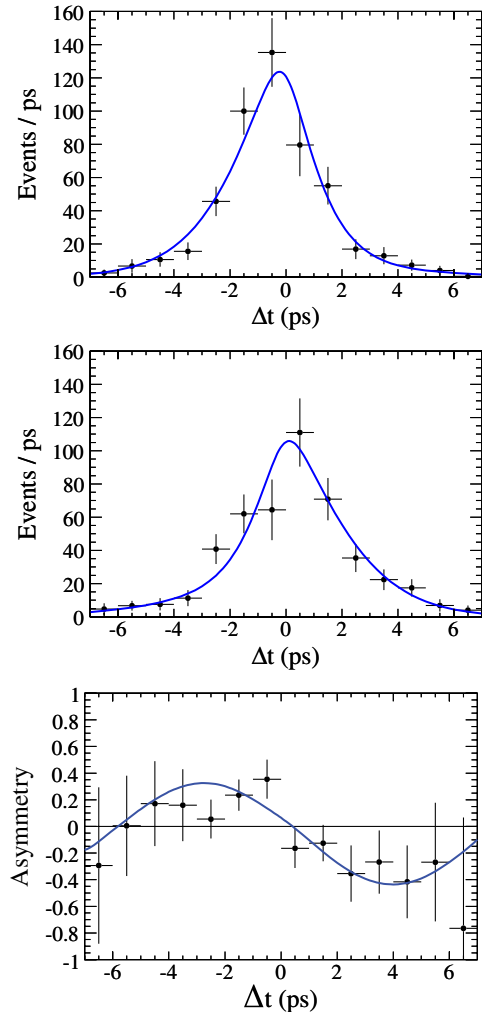


FIG. 5 (color online). \mathcal{P} lots of the Δt distributions for signal $\pi^+ \pi^-$ events tagged as (top) B^0 or (middle) \bar{B}^0 , and (bottom) their asymmetry $a(\Delta t)$, from Eq. (1). The points with error bars show the data, and the lines represent the PDFs used in the fit and reflect the fit result.

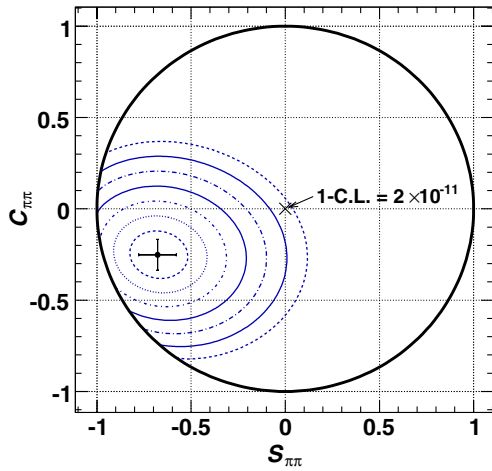


FIG. 6 (color online). $S_{\pi^+\pi^-}$ and $C_{\pi^+\pi^-}$ in $B^0 \rightarrow \pi^+\pi^-$ decays showing the central values (point with error bars) and statistical confidence-level (C.L.) contours for $1 - \text{C.L.} = 0.317$ (1σ), 4.55×10^{-2} (2σ), 2.70×10^{-3} (3σ), 6.33×10^{-5} (4σ), 5.73×10^{-7} (5σ), 1.97×10^{-9} (6σ), and 2.56×10^{-12} (7σ) calculated from the square root of the change in the value of $-2 \ln \mathcal{L}$ with respect to its value at the minimum. The unit circle represents the physical region $S_{\pi^+\pi^-}^2 + C_{\pi^+\pi^-}^2 \leq 1$.

MC events and parametrized experiments to test for a potential bias in the fit, for which we estimate an uncertainty of 0.001.

Systematic uncertainties for the CP asymmetries $S_{\pi^+\pi^-}$ and $C_{\pi^+\pi^-}$ are listed in Table IV. The largest uncertainties on $S_{\pi^+\pi^-}$ are due to the Δt and B -flavor-tagging parameters, and are determined by varying the Δt resolution function parameters and the flavor-tagging parameters by their uncertainties. The largest $C_{\pi^+\pi^-}$ uncertainty is due to the effect of CP violation in the B_{tag} decays [40]. The effect of SVT misalignment is determined by reconstructing events with shifted alignment parameters, and the uncertainties due to the machine boost and detector size are obtained by scaling Δt by 1.0046. We evaluate uncertainties due to the measurement of the beam spot by shifting its position in the vertical direction by $20 \mu\text{m}$, and those due to the knowledge of

TABLE III. Summary of systematic uncertainties on $\mathcal{A}_{K^-\pi^+}$. To address the $\mathcal{A}_{K^-\pi^+}$ bias due to hadronic interactions of charged kaons with the detector material, we shift the $\mathcal{A}_{K^-\pi^+}$ value obtained in the fit by $+0.005$.

Source	$\mathcal{A}_{K^-\pi^+}$
Material interactions	$+0.005 -0.003$
θ_C and dE/dx PDFs	0.002
Alternative DIRC parametrization	0.002
Potential bias	0.001
Total	$+0.006 -0.004$

TABLE IV. Summary of systematic uncertainties on $S_{\pi^+\pi^-}$ and $C_{\pi^+\pi^-}$.

Source	$S_{\pi^+\pi^-}$	$C_{\pi^+\pi^-}$
DIRC θ_C	0.0064	0.0050
DCH dE/dx	0.0032	0.0037
Signal Δt	0.0199	0.0055
SVT local alignment	0.0004	0.0002
Boost/detector z size	0.0021	0.0013
PEP-II beam spot	0.0028	0.0014
B -flavor tagging	0.0146	0.0138
$\Delta m_d, \tau_{B^0}$ [29]	0.0004	0.0017
Potential bias	0.0041	0.0043
CP violation in B_{tag} decays	0.007	0.016
Total	0.027	0.023

the $B^0 - \bar{B}^0$ mixing frequency and the B^0 lifetime are determined by varying these parameters within their uncertainties [29]. The uncertainties due to particle identification and potential fit bias are evaluated as described above for $\mathcal{A}_{K^-\pi^+}$.

B. $B^0 \rightarrow \pi^0\pi^0$ results

Results from the ML fit for the $B^0 \rightarrow \pi^0\pi^0$ decay mode are summarized in Table V. s Plots of m_{ES} , ΔE , and NN for $B^0 \rightarrow \pi^0\pi^0$ are shown in Fig. 7, and for the $q\bar{q}$ background in Fig. 8.

The various systematic uncertainties for the $B^0 \rightarrow \pi^0\pi^0$ decay mode are listed in Tables VI and VII. The uncertainty in the efficiency is dominated by a 3% systematic uncertainty per π^0 , which is estimated from a study of $\tau \rightarrow \pi\pi^0\nu_\tau$ decays. An uncertainty of 1.0% is due to the resolution of the signal shape, and an additional uncertainty of 0.5% is due to the limited knowledge of the m_{ES} and ΔE peak positions in data. These are estimated by shifting the m_{ES} and ΔE means and resolutions by amounts determined from MC-data comparison in a control sample of $B^+ \rightarrow \pi^+\pi^0$ events. An uncertainty of 1.5%, which is determined from the B_{flav} sample, is due to the $|\cos\theta_S|$ requirement. A 1.1% uncertainty is assigned to the number of $B\bar{B}$ events in the data sample. Systematic uncertainties involving the ML fit are evaluated by varying the PDF parameters and refitting the data. These contribute an uncertainty of 8.3 events to the branching-fraction measurement and an uncertainty of 0.055 to $C_{\pi^0\pi^0}$.

C. $B^0 \rightarrow K_S^0\pi^0$ results

The efficiency and branching fraction measured for the $B^0 \rightarrow K_S^0\pi^0$ decay mode are summarized in Table V (CP -violation parameters have been reported in Ref. [4]).

We show s Plots of m_{miss} , m_B , L_2/L_0 , and $\cos\theta_B^*$ for signal events in Fig. 9 and for background events in Fig. 10.

TABLE V. Results for the $B^0 \rightarrow \pi^0 \pi^0$ and $B^0 \rightarrow K_S^0 \pi^0$ decay modes. For each mode, we show the signal yield N_{sig} , the efficiency, the branching fraction, and the CP -violation parameter C . When two uncertainties are given, the first is statistical and the second is systematic. Uncertainties for the signal yields are statistical, and those for the efficiencies are systematic.

	N_{sig}	Efficiency (%)	Branching fraction (10^{-6})	C
$B^0 \rightarrow \pi^0 \pi^0$	247 ± 29	28.8 ± 1.8	$1.83 \pm 0.21 \pm 0.13$	$-0.43 \pm 0.26 \pm 0.05$
$B^0 \rightarrow K_S^0 \pi^0$	556 ± 32	34.2 ± 1.2	$5.1 \pm 0.3 \pm 0.2$	

The systematic uncertainties on the branching fraction $\mathcal{B}(B^0 \rightarrow K_S^0 \pi^0)$ are summarized in Table VIII. The uncertainty on the efficiency of the K_S^0 reconstruction is obtained from detailed comparison of inclusive K_S^0 candidates in data and MC. The π^0 efficiency uncertainty is evaluated from the ratio of branching fractions $\mathcal{B}(D^0 \rightarrow K^- \pi^+ \pi^0)/\mathcal{B}(D^0 \rightarrow K^- \pi^+)$. To compute the systematic uncertainty associated with the statistical precision on the parameters of the likelihood function, we shift each parameter by its associated uncertainty and repeat the fit. For

Δt and the tagging parameters, the uncertainty is obtained from the fit to the B_{flav} sample, while for the other parameters it is obtained from MC. This uncertainty accounts for the size of the sample used for determining the shape of the likelihood function in Eq. (9). A systematic uncertainty associated with the data-MC agreement in the shape of the signal PDFs is evaluated by taking the largest deviation observed when the parameters of the individual signal PDFs for m_{miss} , m_B , L_2/L_0 , and $\cos \theta_B^*$ are allowed to vary in the fit. The output values of the PDF parameters

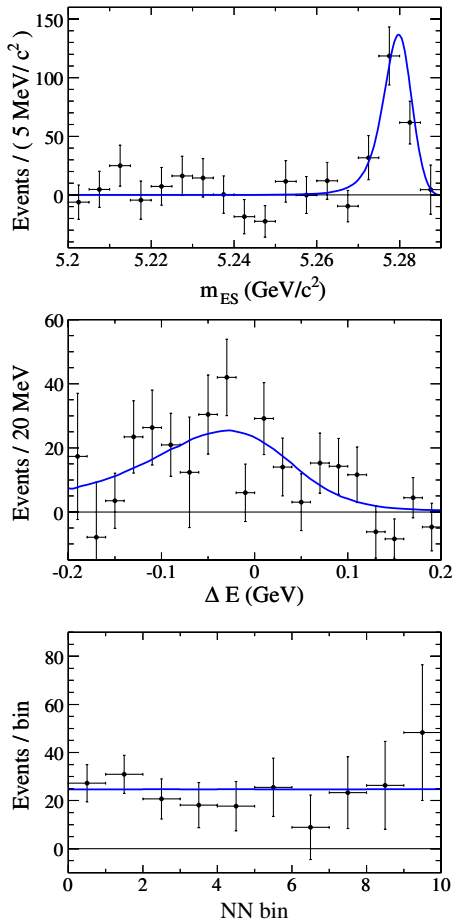


FIG. 7 (color online). $B^0 \rightarrow \pi^0 \pi^0$ signal plots with background subtracted using the $s\mathcal{P}$ lots technique. From top to bottom: m_{ES} , ΔE , and NN . The points with error bars show the data, and the line in each plot shows the corresponding PDF.

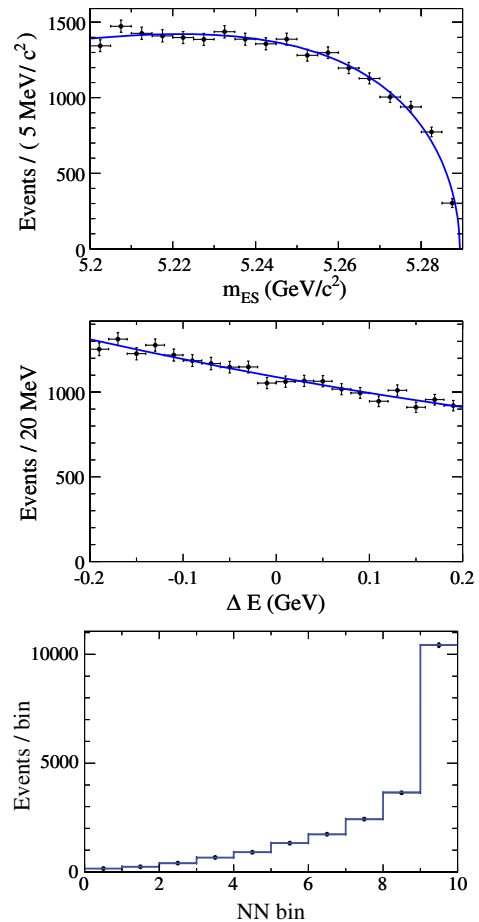


FIG. 8 (color online). $B^0 \rightarrow \pi^0 \pi^0$ background plots with signal subtracted using the $s\mathcal{P}$ lots technique. From top to bottom: m_{ES} , ΔE , and NN . The points with error bars show the data, and the line in each plot shows the corresponding PDF.

TABLE VI. Systematic uncertainties on the $B^0 \rightarrow \pi^0 \pi^0$ signal yield $N_{\pi^0 \pi^0}$ and direct CP asymmetry $C_{\pi^0 \pi^0}$. The total uncertainty is the sum in quadrature of the individual uncertainties.

Source	$N_{\pi^0 \pi^0}$	$C_{\pi^0 \pi^0}$
Peaking background	4.9	0.030
Tagging	0.35	0.034
Background shape	5.5	0.023
Signal shape	3.8	0.020
Total fit systematic uncertainty	8.3	0.055

are also used to assign a systematic uncertainty to the efficiency of the event selection requirements on the likelihood variables, by comparing the efficiency in the data to that in the MC. We evaluate the systematic uncertainty due to the neglected correlations among fit variables using a set of MC experiments, in which we embed signal events from a full detector simulation with events generated from the background PDFs. Since the shifts are small and only marginally significant, we use the average relative shift in the yield as the associated systematic uncertainty.

In the fit we neglect background from B decays, which is estimated from simulation to contribute of order 0.1% of the total background. To account for a bias due to this, we study in detail the effect of a number of specific B decay channels that dominate this type of background, notably $B^+ \rightarrow \rho^+ K_S^0$, $B^+ \rightarrow K^{*+} \pi^0$, and $B^+ \rightarrow K_S^0 \pi^0 \pi^+$. We embed these simulated B -background events in the data set and find the average shift in the fit signal yield to be +5.2 events. We adjust the signal yield accordingly and use half of the bias as a systematic uncertainty.

For the branching fraction, additional systematic uncertainties originate from the uncertainty on the selection efficiency, the number of $B\bar{B}$ pairs in the data sample (1.1%), and the branching fractions $\mathcal{B}(K_S^0 \rightarrow \pi^+ \pi^-)$ and $\mathcal{B}(\pi^0 \rightarrow \gamma\gamma)$ [29].

TABLE VII. Relative systematic uncertainties on the $B^0 \rightarrow \pi^0 \pi^0$ branching fraction. The total uncertainty is the sum in quadrature of the relative uncertainties on the signal yield (from Table VI), the signal efficiency, and the number of $B\bar{B}$ pairs.

Source	$\mathcal{B}(B^0 \rightarrow \pi^0 \pi^0)$
Signal yield syst. uncertainty	3.4%
π^0 efficiency	6.0%
$ \cos \theta_S $ selection	1.5%
Neutrals resolution	1.0%
m_{ES} and ΔE shape	0.5%
Number of $B\bar{B}$ pairs	1.1%
Total systematic uncertainty	7.2%

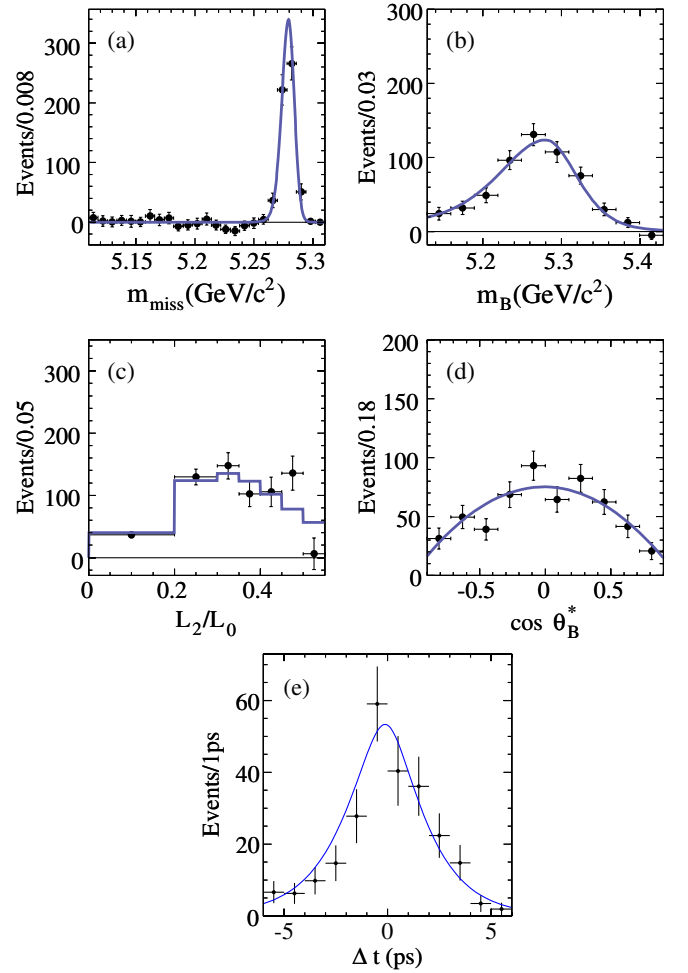


FIG. 9 (color online). s Plots of the (a) m_{miss} , (b) m_B , (c) L_2/L_0 , (d) $\cos \theta_B^*$, and (e) Δt distributions for signal events in the $B^0 \rightarrow K_S^0 \pi^0$ sample. The points with error bars represent the data, and the lines show the shapes of signal PDFs as obtained from the ML fit.

V. RESULTS FOR $\Delta\alpha_{\pi\pi}$ AND α

We combine our results for $\mathcal{B}(B^0 \rightarrow \pi^0 \pi^0)$ with the branching fractions $\mathcal{B}(B^0 \rightarrow \pi^+ \pi^-) = (5.5 \pm 0.4 \pm 0.3) \times 10^{-6}$ and $\mathcal{B}(B^\pm \rightarrow \pi^\pm \pi^0) = (5.02 \pm 0.46 \pm 0.29) \times 10^{-6}$ previously measured by *BABAR* [6,15] to evaluate the constraints on both the penguin contribution to α and on the CKM angle α itself. Constraints are evaluated by scanning the parameters $|\Delta\alpha_{\pi\pi}|$ and α , and then calculating the χ^2 for the five amplitudes (A^{+0} , A^{+-} , A^{00} , \bar{A}^{+-} , \bar{A}^{00}) from our measurements and the isospin-triangle relations [10]. Each χ^2 value is converted to a confidence level, which is shown in Fig. 11 for $\Delta\alpha_{\pi\pi}$ and α . The α plot exhibits six clear peaks, a result of the eightfold trigonometric ambiguity in the extraction of α and the fact that two pairs of peaks are nearly merged. The upper bound on $|\Delta\alpha_{\pi\pi}|$ is 43° at the 90% C.L., and the range $[23^\circ, 67^\circ]$ in α is excluded at the 90% C.L. The point

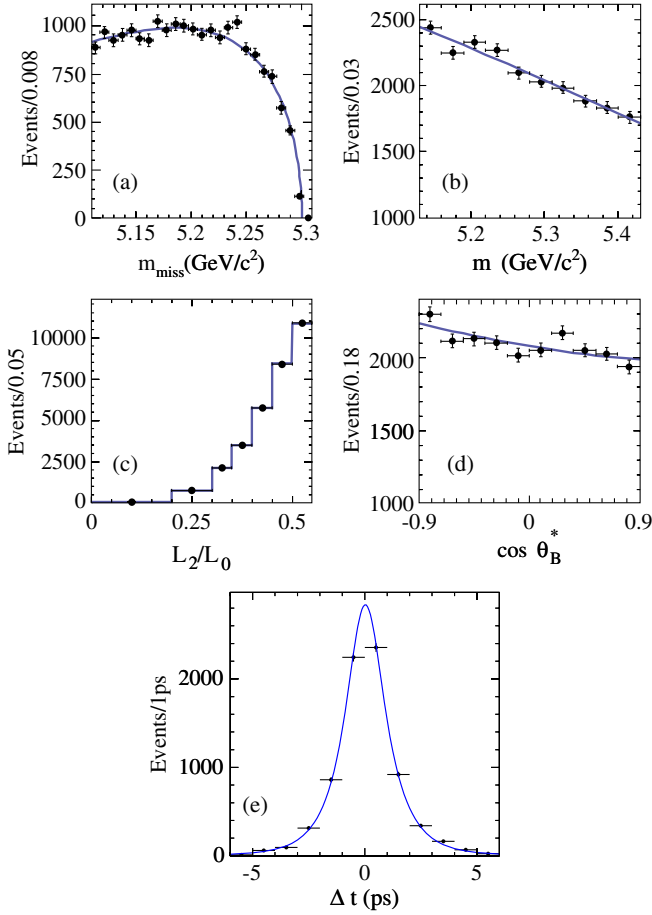


FIG. 10 (color online). \mathcal{P} lots of the (a) m_{miss} , (b) m_B , (c) L_2/L_0 , (d) $\cos \theta_B^*$, and (e) Δt distributions for background events in the $B^0 \rightarrow K_S^0 \pi^0$ sample. The points with error bars represent the data, and the lines show the shapes of signal PDFs as obtained from the ML fit.

$\alpha = 0$, which corresponds to no CP violation, and the values of α near 0 or π can be excluded with additional physics input [6,41]. If we consider only the solution preferred in the SM [42], α lies in the range $[71^\circ, 109^\circ]$

TABLE VIII. Summary of dominant contributions to the systematic uncertainty on the measurement of $\mathcal{B}(B^0 \rightarrow K_S^0 \pi^0)$.

Source	$\sigma(\mathcal{B}(B^0 \rightarrow K_S^0 \pi^0))(\%)$
π^0 efficiency	3.0
K_S^0 efficiency	0.5
Selection criteria	1.5
PDF-parameters precision	0.22
Shape of signal PDFs	0.45
$B\bar{B}$ background	0.47
Correlations	0.40
Resolution function	0.49
Number of $B\bar{B}$ pairs	1.1
Total	3.7

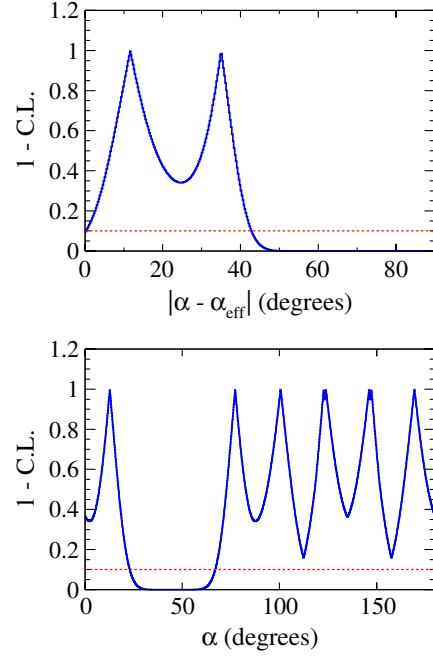


FIG. 11 (color online). (Top) Constraint on $\Delta\alpha_{\pi\pi} = \alpha - \alpha_{\text{eff}}$ expressed as one minus the confidence level as a function of $|\Delta\alpha_{\pi\pi}|$. We find an upper bound on $|\Delta\alpha_{\pi\pi}|$ of 43° at the 90% C.L. (Bottom) constraint on the CKM angle α . We exclude the range $[23^\circ, 67^\circ]$ in α at the 90% C.L. Only the isospin-triangle relations and the expressions in Eq. (1) are used in this constraint.

at the 68% C.L. This is consistent with the more restrictive constraints on α obtained from analysis of the $B \rightarrow \rho\rho$ system [43], as well as those from $B^0 \rightarrow (\rho\pi)^0$ [44] and $B^0 \rightarrow a_1\pi$ [45].

VI. CONCLUSIONS

We measure the CP -asymmetry parameters

$$S_{\pi^+\pi^-} = -0.68 \pm 0.10 \pm 0.03,$$

$$C_{\pi^+\pi^-} = -0.25 \pm 0.08 \pm 0.02,$$

$$\mathcal{A}_{K^-\pi^+} = -0.107 \pm 0.016^{+0.006}_{-0.004},$$

$$C_{\pi^0\pi^0} = -0.43 \pm 0.26 \pm 0.05,$$

and CP -averaged branching fractions

$$\mathcal{B}(B^0 \rightarrow \pi^0\pi^0) = (1.83 \pm 0.21 \pm 0.13) \times 10^{-6},$$

$$\mathcal{B}(B^0 \rightarrow K^0\pi^0) = (10.1 \pm 0.6 \pm 0.4) \times 10^{-6}.$$

We find a 68% C.L. region for α of $[71^\circ, 109^\circ]$ and exclude values in the range $[23^\circ, 67^\circ]$ at the 90% C.L. We observe direct CP violation in $B^0 \rightarrow K^+\pi^-$ with a significance of 6.1σ and in $B^0 \rightarrow \pi^+\pi^-$ with a significance of 6.7σ , including systematic uncertainties. Ignoring color-suppressed tree amplitudes, the charge asymmetries in

$K^+ \pi^-$ and $K^+ \pi^0$ should be equal [21], which is not supported by recent *BABAR* and Belle data [5,6,46]. These results might indicate a large color-suppressed amplitude, an enhanced electroweak penguin, or possibly new-physics effects [47].

Our result for $\mathcal{B}(B^0 \rightarrow K^0 \pi^0)$ is consistent with the sum-rule prediction [21,22] $\mathcal{B}(K^0 \pi^0)^{\text{sr}} = \frac{1}{2}(\mathcal{B}(K^+ \pi^-) + \frac{\tau_0}{\tau_+}[\mathcal{B}(K^0 \pi^+) - 2\mathcal{B}(K^+ \pi^0)]) = (8.4 \pm 0.8) \times 10^{-6}$ obtained using the currently published results [6,15–18] for the three $B \rightarrow K\pi$ rates on the right-hand side of this equation and the lifetimes τ_+ and τ_0 of the charged and neutral B mesons.

The results presented here supersede those of our prior publications [5–7].

ACKNOWLEDGMENTS

We are grateful for the extraordinary contributions of our PEP-II colleagues in achieving the excellent luminosity and machine conditions that have made this work possible. The

success of this project also relies critically on the expertise and dedication of the computing organizations that support *BABAR*. The collaborating institutions wish to thank SLAC for its support and the kind hospitality extended to them. This work is supported by the U.S. Department of Energy and National Science Foundation, the Natural Sciences and Engineering Research Council (Canada), the Commissariat à l’Energie Atomique and Institut National de Physique Nucléaire et de Physique des Particules (France), the Bundesministerium für Bildung und Forschung and Deutsche Forschungsgemeinschaft (Germany), the Istituto Nazionale di Fisica Nucleare (Italy), the Foundation for Fundamental Research on Matter (The Netherlands), the Research Council of Norway, the Ministry of Education and Science of the Russian Federation, Ministerio de Ciencia e Innovación (Spain), and the Science and Technology Facilities Council (United Kingdom). Individuals have received support from the Marie-Curie IEF program (European Union) and the A. P. Sloan Foundation (U.S.).

-
- [1] A. B. Carter and A. I. Sanda, *Phys. Rev. Lett.* **45**, 952 (1980); M. Bander, D. Silverman, and A. Soni, *Phys. Rev. Lett.* **43**, 242 (1979).
- [2] N. Cabibbo, *Phys. Rev. Lett.* **10**, 531 (1963); M. Kobayashi and T. Maskawa, *Prog. Theor. Phys.* **49**, 652 (1973).
- [3] B. Aubert *et al.* (*BABAR* Collaboration), *Phys. Rev. D* **79**, 072009 (2009); K.-F. Chen *et al.* (Belle Collaboration), *Phys. Rev. Lett.* **98**, 031802 (2007); H. Sahoo *et al.* (Belle Collaboration), *Phys. Rev. D* **77**, 091103 (2008).
- [4] B. Aubert *et al.* (*BABAR* Collaboration), *Phys. Rev. D* **79**, 052003 (2009).
- [5] B. Aubert *et al.* (*BABAR* Collaboration), *Phys. Rev. Lett.* **99**, 021603 (2007).
- [6] B. Aubert *et al.* (*BABAR* Collaboration), *Phys. Rev. D* **76**, 091102 (2007).
- [7] B. Aubert *et al.* (*BABAR* Collaboration), *Phys. Rev. D* **77**, 012003 (2008).
- [8] H. Ishino *et al.* (Belle Collaboration), *Phys. Rev. Lett.* **98**, 211801 (2007).
- [9] M. Fujikawa *et al.* (Belle Collaboration), *Phys. Rev. D* **81**, 011101 (2010).
- [10] J. Charles, A. Höcker, H. Lacker, S. Laplace, F. R. Diberder, J. Malcés, J. Ocariz, M. Pivk, and L. Roos (The CKMfitter Group), *Eur. Phys. J. C* **41**, 1 (2005).
- [11] M. Bona *et al.* (UTfit Collaboration), *J. High Energy Phys.* **07** (2005) 028.
- [12] M. Bona *et al.* (UTfit Collaboration), *Phys. Rev. Lett.* **97**, 151803 (2006); M. Bona *et al.* (UTfit Collaboration), *J. High Energy Phys.* **03** (2008) 049.
- [13] M. Gronau and D. London, *Phys. Rev. Lett.* **65**, 3381 (1990).
- [14] M. Beneke and M. Neubert, *Nucl. Phys.* **B675**, 333 (2003); C. W. Bauer, D. Pirjol, I. Z. Rothstein, and I. W. Stewart, *Phys. Rev. D* **70**, 054015 (2004); M. Ciuchini, E. Franco, G. Martinelli, M. Pierini, and L. Silvestrini, *Phys. Lett. B* **515**, 33 (2001).
- [15] B. Aubert *et al.* (*BABAR* Collaboration), *Phys. Rev. D* **75**, 012008 (2007).
- [16] B. Aubert *et al.* (*BABAR* Collaboration), *Phys. Rev. Lett.* **97**, 171805 (2006).
- [17] K. Abe, K. Taniguchi, S. Ohtani, T. Takenobu, Y. Iwasa, and T. Arima (Belle Collaboration), *Phys. Rev. Lett.* **98**, 181804 (2007); **99**, 121601 (2007).
- [18] A. Bornheim *et al.* (CLEO Collaboration), *Phys. Rev. D* **68**, 052002 (2003); **75**, 119907(E) (2007).
- [19] A. J. Buras and R. Fleischer, *Eur. Phys. J. C* **16**, 97 (2000); A. J. Buras, R. Fleischer, S. Recksiegel, and F. Schwab, *Phys. Rev. Lett.* **92**, 101804 (2004); *Nucl. Phys.* **B697**, 133 (2004).
- [20] M. Gronau and J. L. Rosner, *Phys. Lett. B* **572**, 43 (2003); T. Yoshikawa, *Phys. Rev. D* **68**, 054023 (2003); V. Barger, C. W. Chiang, P. Langacker, and H. S. Lee, *Phys. Lett. B* **598**, 218 (2004); S. Mishima and T. Yoshikawa, *Phys. Rev. D* **70**, 094024 (2004); Y.-L. Wu and Y.-F. Zhou, *Phys. Rev. D* **71**, 021701 (2005).
- [21] M. Gronau and J. L. Rosner, *Phys. Rev. D* **59**, 113002 (1999).
- [22] M. Gronau, *Phys. Lett. B* **627**, 82 (2005); H. J. Lipkin, *Phys. Lett. B* **445**, 403 (1999); C. W. Bauer, I. Z. Rothstein, and I. W. Stewart, *Phys. Rev. D* **74**, 034010 (2006).
- [23] B. Aubert *et al.* (*BABAR* Collaboration), *Nucl. Instrum. Methods Phys. Res., Sect. A* **479**, 1 (2002).
- [24] M. Kocian, Report No. SLAC-PUB-10170.
- [25] S. Agostinelli *et al.* (Geant4 Collaboration), *Nucl. Instrum. Methods Phys. Res., Sect. A* **506**, 250 (2003).
- [26] T. Sjöstrand, *Comput. Phys. Commun.* **82**, 74 (1994).

- [27] D. J. Lange, *Nucl. Instrum. Methods Phys. Res., Sect. A* **462**, 152 (2001).
- [28] The use of charge-conjugate modes is implied throughout this paper unless otherwise noted.
- [29] K. Nakamura *et al.* (Particle Data Group), *J. Phys. G* **37**, 075021 (2010).
- [30] J. D. Bjorken and S. J. Brodsky, *Phys. Rev. D* **1**, 1416 (1970).
- [31] G. C. Fox and S. Wolfram, *Phys. Rev. Lett.* **41**, 1581 (1978).
- [32] S. Brandt, Ch. Peyrou, R. Sosnowski, and A. Wroblewski, *Phys. Lett.* **12**, 57 (1964); E. Farhi, *Phys. Rev. Lett.* **39**, 1587 (1977).
- [33] B. Aubert *et al.* (BABAR Collaboration), *Phys. Rev. Lett.* **94**, 161803 (2005).
- [34] We use the shorthand notation ρ and a_1 to refer to the $\rho(770)$ and $a_1(1260)$, respectively.
- [35] B. Aubert *et al.* (BABAR Collaboration), *Phys. Rev. D* **66**, 032003 (2002).
- [36] The function is $f(x) \propto x\sqrt{1-x^2} \exp[-\zeta(1-x^2)]$, where the slope ζ is a fit parameter and $x = m_{ES}/E_b^*$; H. Albrecht *et al.* (ARGUS Collaboration), *Z. Phys. C* **48**, 543 (1990).
- [37] B. Aubert *et al.* (BABAR Collaboration), *Phys. Rev. D* **71**, 111102 (2005).
- [38] B. Aubert *et al.* (BABAR Collaboration), *Phys. Rev. D* **77**, 012003 (2008).
- [39] M. Pivk and F. R. Le Diberder, *Nucl. Instrum. Methods Phys. Res., Sect. A* **555**, 356 (2005).
- [40] O. Long, M. Baak, R. N. Cahn, and D. Kirkby, *Phys. Rev. D* **68**, 034010 (2003).
- [41] M. Bona *et al.* (UTfit Collaboration), *Phys. Rev. D* **76**, 014015 (2007).
- [42] M. Gronau and J. L. Rosner, *Phys. Lett. B* **651**, 166 (2007).
- [43] B. Aubert *et al.* (BABAR Collaboration), *Phys. Rev. Lett.* **97**, 261801 (2006); *Phys. Rev. D* **76**, 052007 (2007); **78**, 071104 (2008); *Phys. Rev. Lett.* **102**, 141802 (2009); C. C. Chiang *et al.* (Belle Collaboration), *Phys. Rev. D* **78**, 111102 (2008).
- [44] B. Aubert *et al.* (BABAR Collaboration), *Phys. Rev. D* **76**, 012004 (2007).
- [45] B. Aubert *et al.* (BABAR Collaboration), *Phys. Rev. D* **81**, 052009 (2010).
- [46] S. W. Lin *et al.* (Belle Collaboration), *Nature (London)* **452**, 332 (2008).
- [47] W. S. Hou, M. Nagashima, and A. Soddu, *Phys. Rev. Lett.* **95**, 141601 (2005); R. Fleischer, S. Recksiegel, and F. Schwab, *Eur. Phys. J. C* **51**, 55 (2007).